International Journal of Remote Sensing
Vol. 26, No. 13, 10 July 2005, 2715–2729

Taylor & Francis
Taylor & Francis Group

InSAR time series analysis of the 9 July 1998 Azores earthquake

C. CATITA†, K. L. FEIGL‡, J. CATALÃO†, J. M. MIRANDA§ and L. M. VICTOR§

†Dep. Matemática/LATTEX, Faculdade de Ciências da Universidade de Lisboa, Ed. C6, Piso 2, 1749-016 Lisboa, Portugal; e-mail: cmcatita@fc.ul.pt

‡Centre National de la Recherche Scientifique, 14 Avenue E. Belin, 31400 Toulouse, France; e-mail: Kurt.Feigl@cnes.fr

§Centro de Geofísica da Universidade de Lisboa, FCUL, Ed. C8, 1749-016 Lisboa, Portugal; e-mail: jmiranda@fc.ul.pt

(*Received 4 March 2004; in final form 22 October 2004*)

The 9 July 1998 M_w 6.1 Pico-Faial earthquake was one of the largest events recorded in the Azores (North Atlantic) in recent years. It generated significant co-seismic deformation that was captured by a GPS network on Faial Island. On the other islands, where no such networks were available, the co-seismic surface displacement field was heretofore unknown. To measure it on Pico Island, we analysed Synthetic Aperture Radar (SAR) images using interferometry. Our dataset includes 17 images acquired by the ERS-1 and ERS-2 satellites in descending passes between June 1992 and November 2000. The interferograms computed from the available image pairs show poor correlation, particularly over the dense vegetated area of Faial Island and the flanks of Pico Volcano. However, a well-correlated fringe pattern remains over 33 months for barren parts of NW Pico Island. We analysed phase profiles across this fringe to distinguish the relative contributions of the co-seismic signal and the tropospheric noise, observing a co-seismic step of 29 ± 10 mm in range.

1. Introduction

On 9 July 1998 at 05:19:15 GMT, an earthquake (M_w 6.1) occurred near Faial Island (Azores Archipelago, Portugal) with the epicentre 10 km offshore to the NE of the coast (figure 1). This earthquake was strongly felt in Pico where some buildings were partially destroyed. The seismic shaking triggered many damaging landslides (Madeira *et al.* 1998, Gaspar *et al.* 1998). The epicentre computed by the Sistema de Vigilância Sismológica dos Açores (SIVISA) was $38^\circ 38.05' \pm 2.2'$ N, $28^\circ 31.38' \pm 3.4'$ E (Senos *et al.* 1998). Since the earthquake source was offshore, there are no direct observations of surface rupture geometry or slip. Its maximum intensity on the Modified Mercalli scale was VIII in the NE part of Faial and VII in the NW part of Pico Island (Senos *et al.* 1998).

Fernandes *et al.* (2002) analysed Global Positioning System (GPS) data acquired in 1993, 1994, 1997 and 1999 on FAIM site in the SE of Faial (see figure 1 for location), complemented by a dense network of 30 stations well distributed over Faial Island, which were observed before (10 July to 4 August 1997) and after (5 August to 9 August 1998) the earthquake. This dataset determined the displacement field in Faial. The maximum horizontal amplitude was observed in the NE of the island and reached 8 ± 1.5 cm in south-west direction. According to

International Journal of Remote Sensing
ISSN 0143-1161 print/ISSN 1366-5901 online © 2005 Taylor & Francis Group Ltd
http://www.tandf.co.uk/journals
DOI: 10.1080/01431160512331337835

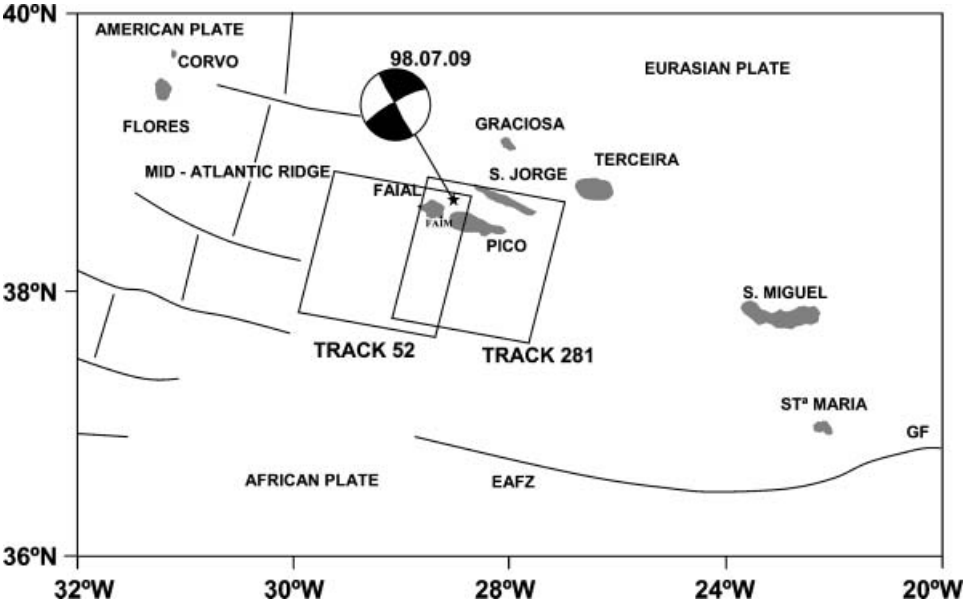

Figure 1. Azores Archipelago, Atlantic North. Gloria fault (GF), East Azores Fracture Zone (EAFZ) and Mid-Atlantic Ridge (MID) are the major geological structures close to the triple junction point where North American, Eurasian and African plates meet. The star identifies the epicentre, at N38.63°, W28.52 determined by SIVISA, and FAIM the site location where meteorological measurements were acquired. The focal mechanism generated by Pico-Faial earthquake of 9 July 1998 is also indicated. Large boxes highlight Synthetic Aperture Radar (SAR) coverage from ERS-1/2.

Fernandes *et al.* (2002), the co-seismic displacement field over Faial can be explained effectively by a simple half space elastic model, considering two basic solutions: one corresponding to a dextral strike slip (Model 1) and the other corresponding to a left lateral strike slip (Model 2). Table 1 summarizes the source parameters determined from the inversion of the geodetic data presented by Fernandes *et al*. (2002). Each of the solutions agrees with one of the focal planes in the centroid moment tensor (Dziewonski *et al*. 1999). Distinguishing between them is challenging because a short offshore fault generates only small gradients in displacement on the islands where the geodetic measurements are located.

Table 1. Two possible solutions (Model 1 and Model 2) of the source parameters determined from inversion of the geodetic data (Fernandes *et al*. 2002).

Model	Model 1: N253E	Model 2: N165E
Lat. (°)	38°37′06.1″ ± 08.1″ N	38°36′57.0″ ± 08.6″ N
Long. (°)	28°32′25.9″ ± 20.9″ W	28°33′22.2″ ± 19.3″ W
Strike (°)	253 ± 0.8	165 ± 0.8
Depth (m)	1970 ± 94	1948 ± 97
Length (m)	9500 ± 411	9326 ± 214
Width (m)	4656 ± 428	4248 ± 468
Dip (°)	82	89
Slip (m)	− 0.98 ± 0.08	1.04 ± 0.09
Rake (°)	− 180	− 8
M0 ($\times 10^{18}$ Nm)	1.30 ± 0.31	1.24 ± 0.19

On Pico Island, however, no dense GPS arrays existed before the 1998 earthquake. Consequently, Synthetic Aperture Radar (SAR) images acquired by the ERS-1 and ERS-2 satellites constitute the best survey available on Pico before the quake. Analysing them with interferometry (InSAR) is the subject of this paper. Other InSAR studies of earthquakes are well documented in the literature (Massonnet *et al.* 1993, Feigl *et al.* 1995, Massonnet and Feigl 1995a, Murakami *et al.* 1996, Klinger *et al.* 2000, Sandwell *et al.* 2000, Wright *et al.* 2001, Nishimura *et al.* 2001, Feigl 2002). InSAR measures the phase difference between two radar images collected on successive passes over the same area (e.g. Massonnet and Feigl 1998). The resulting interference pattern maps change in range along the line-of-sight (LOS) from the satellite to the ground. Each fringe represents half a wavelength of range change, or 28-mm for the C-band ERS satellites.

2. SAR data and interferometric analysis

To select ERS images around the time of the earthquake from the archives of the European Space Agency (ESA), we had to balance several criteria. The number of ERS images suitable for this co-seismic study is limited. ERS acquired fewer images over the Azores archipelago than in other areas of Europe, apparently to avoid switching the powerful radar sensor on and off.

On this study, we applied the two-pass approach described by Massonnet and Feigl (1998) and implemented by the Diapason software developed at French space agency (Centre National d'Etudes Spatiales, CNES). The topographic contribution was compensated using a Digital Elevation Model (DEM) provided by the Portuguese military institute (Instituto Geográfico do Exército), with a 50-m horizontal resolution and average height accuracy better than 5 m (Afonso *et al.* 2002). To reduce uncertainty in the satellite positioning, we used precise orbit trajectories estimated by Delft University (Scharroo and Visser 1998). The signal-to-noise ratio of each interferogram was improved by using a weighted power spectrum filter (Goldstein and Werner 1998).

InSAR works best in arid regions because the ground cover remains unchanged between images (Massonnet *et al.* 1993, Murakami *et al.* 1996, Rosen *et al.* 1996, Sandwell *et al.* 2000). But this is not the case in the Azores, as the vegetation is very dense in most places.

On Faial the observed decorrelation seems to be the consequence of both dense vegetative cover of the island and the long time interval between images. While bare volcanic rocks cover most of Pico Island, Faial has a dense agricultural coverage. Combining these two factors, we are unable to obtain successful interferograms over Faial. A similar problem exists on the Pico central volcano, probably due to slope instabilities.

The image acquisition geometry is also unfavourable for this earthquake on Faial Island. Radar measures scalar change in the satellite-to-ground distance. The change in range is the scalar product of the ground displacement vector and the unit vector pointing from the ground point toward the satellite. The mean unitary vector pointing from the epicentre of the 9 July earthquake towards the satellite, in descending orbits with a coordinate set (east, north, up), has the components (0.39, -0.08, 0.91) and (0.46, -0.09, 0.88) for tracks used on this study (52 and 281, respectively). If we consider the source parameters proposed by Fernandes *et al.* (2002) we can compute a synthetic interferogram, taking into account the actual acquisition geometry. The predicted co-seismic displacements vectors on Faial

Island are almost orthogonal to the satellite line of sight, not detectable by the SAR satellites on the orbital tracks used on this study (figure 2). Notice that on both tracks the acquisition geometry is quite similar, which produces identical synthetic interferograms.

The sparse, uneven nature of the ERS acquisitions constitutes another limiting factor of our dataset. The last image acquired before the 1998 earthquake was on 31 December of 1995, almost three years before this event. In consequence, all the co-seismic interferograms span at least three years and decorrelate badly.

Table 2 shows a set of all SAR images acquired on this study: eight images from track 281, frame 2835 and nine images from track 52, frame 2835. Of the available scenes 13 were acquired before the end of 1995, while only four were acquired after the 1998 event. All scenes were acquired in descending orbits during the day (12:36 UTC).

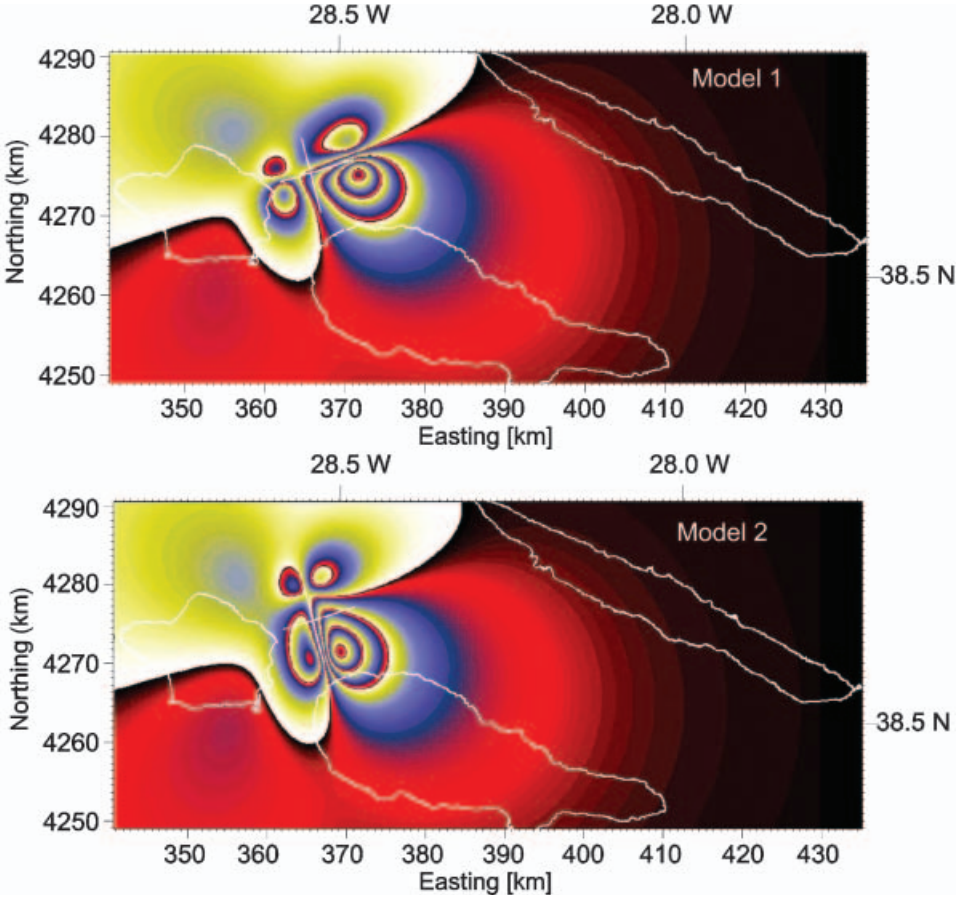

Figure 2. Synthetic interferogram representing fringe pattern computed from source parameters determined by Fernandes *et al.* (2002) (Model 1 and Model 2: solutions described in section 1). Each fringe, in the synthetic interferogram, denotes 28.3 mm of change in range. Colour sequence red-blue-yellow indicates range change increasing and red-yellow-blue range change decreasing. Coordinates are easting and northing in km and the cartographic projection is the Universal Transverse Mercator projection, zone 26.

Table 2. ERS SAR images, of tracks 52 and 281, acquired for this study. Normal baselines are computed considering the images 981011 (track 281) and 980925 (track 52) as reference. Meteorological parameters Temperature (T), Humidity (U) and Pressure (P) were acquired at FAIM station (Horta Island) and the water vapour (Wv) is computed from radiosonda data acquired at Lajes (Terceira Island), at 12 hours of local time on image acquisition date.

Orbit	Sensor	Date	Track	Frame	Normal baseline (m)	P (mb)	T(°C)	U (%)	Wv (mb)
636	ERS2	950604	281	2835	− 470	1026	21	75	14.6
1137	ERS2	950709	281	2835	− 870	1018	21	95	17.3
2640	ERS2	951022	281	2835	546	1009	22	88	22
3141	ERS2	951126	281	2835	− 865	1024	16	66	9.6
23315	ERS1	951230	281	2835	94	997	16	74	10.3
3642	ERS2	951231	281	2835	− 159	995	13	72	10.1
18171	ERS2	981011	281	2835	0	1027	23	77	18.2
29193	ERS2	001119	281	2835	623	1028	21	79	15.7

Orbit	Sensor	Date	Track	Frame	Normal baseline (m)	P (mb)	T(°C)	U (%)	Wv (%)
4706	ERS1	920609	52	2835	− 32	1012	18	60	12
8714	ERS1	930316	52	2835	− 186	1016	16	81	13.7
908	ERS2	950623	52	2835	− 1060	1009	22	88	13.1
22585	ERS1	951109	52	2835	− 34	1027	16	77	11.2
2912	ERS2	951110	52	2835	− 274	1025	16	73	10
23086	ERS1	951214	52	2835	217	1021	16	63	11.7
3413	ERS2	951215	52	2835	− 31	1015	16	71	9.5
16940	ERS2	980717	52	2835	− 1221	1022	23	76	17.3
17942	ERS2	980925	52	2835	0	1018	23	73	18.9

To detect the co-seismic deformation, we could form seven interferograms spanning the earthquake in track 52, and five in track 281 (table 3). Most of these span time intervals longer than a year. In track 281, only two images acquired after the quake are available (981011 orbit 18171 and 001119 orbit 29193). Among the co-seismic interferograms computed in track 281, the pair 951230–001119 decorrelates badly, possibly due to the long time interval between the acquisitions and the large orbital separation. In track 52, only one post seismic image (980925) correlates well with the pre-seismic images of this track. The pair 950623–980717 constitutes an independent co-seismic interferogram of track 52 but unfortunately the post-seismic image 980717 correlates only with the 950623. The pre-seismic interval was studied with five independent interferograms of track 52 and five independent interferograms of track 281, among the 15 possibilities in track 52 and the six possibilities in track 281. We have just one interferogram to evaluate the post-seismic period of track 281, for the post seismic period (981011–001119).

The scarcity of the available dataset illustrates the need for a satellite mission dedicated to systematic and regular SAR acquisitions.

3. Interferometric results

In figure 3 we present a series of eight co-seismic interferograms corresponding to the available tracks. Significant phase variations are clearly visible and cannot be associated with topographic fringes, nor atmospheric disturbances. Interferograms A to F (figure 3) of track 52 share the same post-seismic image 980925, and

Table 3. Interferometric pairs computed on this study. Interferometric pairs are represented by the date of the image acquisitions ($yymmdd_{master}$–$yymmdd_{slave}$). Ha is the altitude of ambiguity of each pair, ΔT is the temporal baseline, in days, and ΔP the pressure differences, in mb. Δ_{tropo} is the differential tropospheric delay determined by radiosonde data at Lajes (Terceira Island). $\Delta\Delta\rho_{ij}$ corresponds to the spatial difference, between the first and last point of profile 4 (figure 5), extracted from the simulated atmosphere interferograms, based on surface meteorological data applied to the model for tropospheric zenith delay (see §3.2).

No.	Interferometric pair	Track	Ha (m)	ΔT (days)	ΔP (mb)	Δ_{Tropo} (mm) (radiosonda)	$\Delta\Delta\rho_{ij}$ (mm)
–	920609–930316	52	63.72	280	− 4	25.8	1.01
–	920609–951109	52	2483.29	1248	− 15	− 4.8	− 1.38
–	920609–951110	52	40.33	1249	− 13	− 1.7	− 1.20
P	920609–951214	52	− 39.37	1283	− 9	38	− 0.83
P	920609–951215	52	− 17385	1284	− 3	43.8	− 0.28
C	920609–980925	52	− 306.54	2299	− 6	− 34.4	− 0.55
P	930316–951109	52	− 65.4	968	− 11	− 30.6	− 2.39
–	930316–951110	52	109.87	969	− 9	− 27.5	− 2.21
–	930316–951214	52	− 24.33	1003	− 5	12.2	− 1.84
–	930316–951215	52	− 63.49	1004	1	18	− 1.29
C	930316–980925	52	− 52.76	2019	− 2	− 60.2	− 1.57
–	951109–951110	52	41	1	2	3.1	0.18
–	951109–951214	52	− 38.75	35	6	42.8	0.55
P	951109–951215	52	− 2172.91	36	12	48.6	1.10
C	951109–980925	52	− 272.86	1051	9	− 29.6	0.82
–	951110–951214	52	− 19.92	34	4	39.7	0.37
P	951110–951215	52	− 40.24	35	10	45.5	0.92
C	951110–980925	52	− 35.64	1050	7	− 32.7	0.64
–	951214–951215	52	39.45	1	6	5.8	0.55
C	951214–980925	52	45.17	1016	3	− 72.4	0.28
C	951215–980925	52	− 312.05	1015	− 3	− 78.2	− 0.28
C	950623–980717	52	58.4	1120	2	− 46.4	0.18
P	950604–951126	281	31.2	175	2	50.6	0.09
–	950604–951230	281	− 21.3	209	29	163.3	2.68
P	950604–951231	281	− 38.5	210	31	139.7	2.87
C	950604–981011	281	− 26	1225	− 1	39.9	− 0.09
P	950709–951126	281	− 363	140	− 6	140.1	− 0.64
P	951022–951230	281	26.74	70	12	140	1.11
C	951022–001119	281	− 151.24	1855	− 19	− 26.9	− 1.76
P	951230–951231	281	47.69	1	2	− 23.6	0.18
C	951230–981011	281	122.6	1016	30	− 123.4	− 2.77
C	951230–001119	281	− 22.72	1786	− 31	− 166.9	− 2.87
C	951231–981011	281	− 78	1015	− 32	− 99.8	− 2.96
O	981011–001119	281	− 19.17	770	− 1	− 43.5	− 0.09

interferograms G and H, of track 281, share also the post-seismic image 981011. The pattern in track 52 resembles that of track 281 in magnitude and location. Yet interferograms A to F are completely independent of interferograms G and H. Considering the northernmost part of Pico Island closest to the epicentre, we can identify almost one fringe (28 mm) on interferograms C, F, G and H. The observed range increase is referred as subsidence. In spite of the high noise level of the other interferograms, they still exhibited the same shaped fringe pattern, but with less than half a fringe. This fringe seems round, smooth and isolated, typical of earthquake deformation, and does not follow contour lines of topographic elevation. The fringe is continuous, without tears, corroborating the absence of co-seismic rupture of the ground surface. Furthermore, no comparable phase signature appears in other

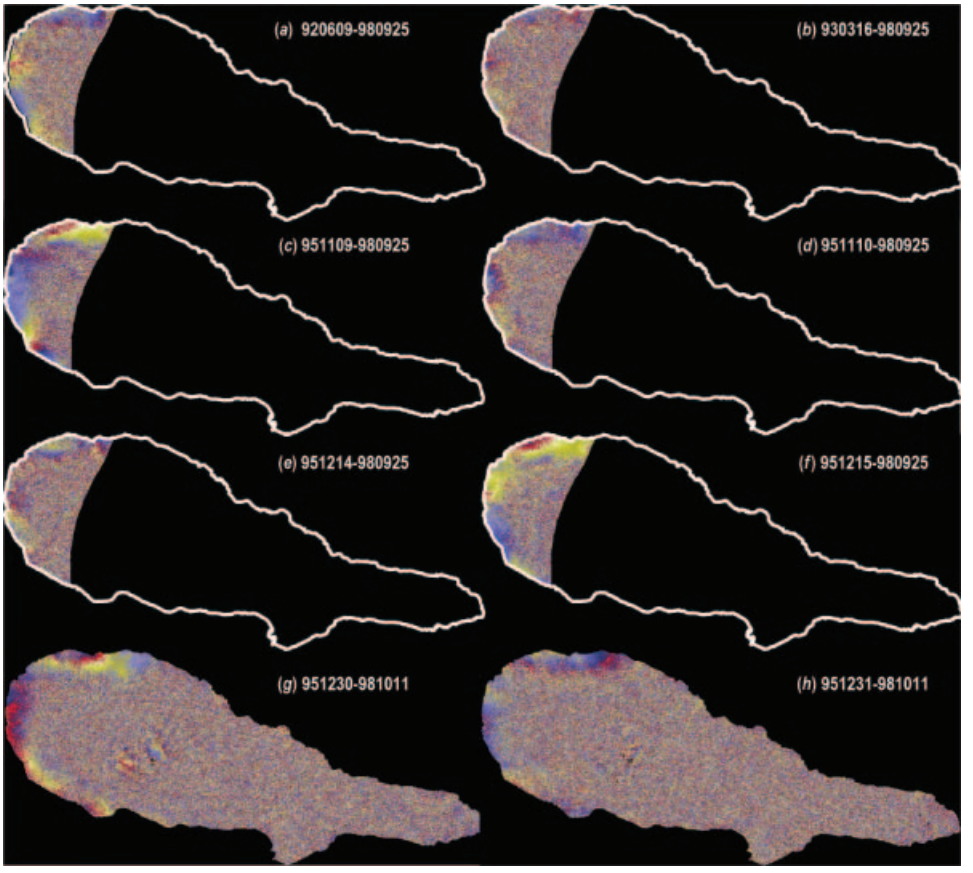

Figure 3. Observed differential co-seismic interferograms. One colour fringe represents 28.3 mm of range change. Panels (*a*) through (*f*): track 52, frame 2835; (*a*): 920609–980925; (*b*): 930316–980925; (*c*): 951109–980925; (*d*): 951110–980925; (*e*): 951214–980925, (*f*): 951215–980925. Panels (*g*) and (*h*): track 281, frame 2835; (*g*): 951230–981011, (*h*): 951231–981011.

parts of Pico Island. For these reasons, we are confident that the observed fringe represents ground deformation caused by the earthquake.

3.1 *Topographic contribution*

The sensitivity of the interferometric pair to the topography is measured by the altitude of ambiguity (Ha), a parameter defined by Massonnet and Rabaute (1993) to quantify the change in altitude needed to produce one topographic fringe. Considering the interferograms of figure 3, we can expect topographic artefacts of magnitude 1/62 cycles or 0.45 mm in range using the best co-seismic pair (interferogram F) and 1/7 cycles of error or 4 mm for the worst co-seismic pair (interferogram D) (see Ha values in table 3). These are negligible even in the worst case. If the observed fringe were a topographic artefact, it would correspond to an error of 35 m in the DEM. Since this value is seven times larger than the DEM's standard deviation, we reject the hypothesis of a topographic artefact. Moreover, the observed signature occurs in an area where the topographic elevation is less than 300 m, making a 35-metre error even less likely. Furthermore, the interferograms

produced using the same DEM spanning a one-day period and worse Ha values, do not show fringes located on the affected area. Therefore, we can conclude that the observed signature in co-seismic interferograms of figure 3 cannot be due to topographic artefacts.

3.2 *Atmospheric contribution*

The atmospheric heterogeneities perturbing the radar signals propagating through the atmosphere are still the prime limitation for the interpretation of interferograms (Goldstein 1995, Massonnet and Feigl 1995b, Tarayre and Massonnet 1996, Delacourt *et al.* 1997, Zebker *et al.* 1997, Hanssen *et al.* 1999, Hanssen 2001).

The atmosphere can be divided into two layers, which have different refractive properties: ionosphere and neutral atmosphere (from now on referred to as troposphere, for simplicity). In the ionosphere, the refractive index depends on the total electron content, and in the troposphere, it depends on the temperature, pressure and water content, and consequently on the meteorological conditions of the atmosphere at the time of the imaging. Usually, the troposphere is divided into wet and hydrostatic components. The hydrostatic component, attributable mostly to the dry gases in the atmosphere, depends essentially on surface pressure and can be modelled well using good measurements. The wet component depends essentially on the partial pressure of water vapour, which is especially difficult to model because it is far more spatially variable than the hydrostatic delay.

The dry component of the neutral atmosphere and the ionospheric component have the largest contributions to the total phase delay. Hanssen (1999) adopts the hypothesis that ionospheric effects cause long wavelength variations over a single SAR image than can be neglected at spatial scales of less than about 50 km. On Pico Island, the well-correlated co-seismic parts of interferograms are less than 10 km wide. Consequently, we can exclude ionospheric delay as a main cause for the fringe observed on the NW part of the island.

The dry tropospheric delay changes if the air pressure changes at a given site between epochs. A pressure change of 1 mb yields to about 2.3 mm of range change (Zebker *et al.* 1997). Meteorological data were recorded at the Observatório Princípe Alberto do Mónaco (OPAM), near the FAIM site (Faial Island) at 64 m altitude. For the interferograms in figure 3, the pressure differences recorded at OPAM are described in table 3 (ΔP column). These differences produce absolute range changes of several centimetres in time but they vary little in space. For instance, the pressure variation due to the 370-m difference in altitude between the endpoints of profile 4 (figure 5), is only 0.04 mb, or less than 0.1 mm in range. If the atmospheric pressure (spatial) distribution is the same at both image acquisition times and we assume hydrostatic equilibrium, each image will experience the same phase shift and the interferogram will show no fringes. Consequently, the tropospheric contribution to the range change recorded in the well-correlated part of the interferograms in the NW part of Pico is of the order of a millimetre.

The wet part of the delay depends on the temperature and water vapour content, which vary both spatially and temporally. The magnitude of the temperature effect can be almost neglected when compared with the water vapour pressure signal (Hanssen *et al.* 1999). Yet modelling the wet zenith delay is quite difficult. In a comparison against radiosonde data, Mendes and Langley (1998) found that existing models have a standard deviation of about 3 cm, when driven with

meteorological data. Using meteorological surface measurements acquired at OPAM for our SAR acquisition epochs, we modelled the hydrostatic component using the Saastamoinen (1972) model and the wet component using the Mendes and Langley (2000) model. A simulated interferogram, affected only with a tropospheric error signal, was computed and used to correct the interferograms used on this study. As expected, the correction of the differential total delay ($\Delta\Delta\rho_{ij}$ column of table 3) varies little over the flat NW part of Pico Island where the fringe pattern appears in the co-seismic interferograms, expressing the weak correlation between the modelled tropospheric delay and the topography (elevation) on this area. For example, the correction applied to interferogram 951230–981011 varies between -14.3 cm (at altitude 0 m) and -12.6 cm (at altitude 2338 m) (figure 4). Note that any range change that is constant in space will not produce fringes in the interferograms. In other words, the interferometric range change includes an arbitrary, unknown additive constant. The reliability of those results was confirmed by ray tracing refractive index profiles obtained by radiosonde launched on Terceira Island (about 120 km from NW Pico), half an hour after the acquisition time of our SAR images. In table 3 (column Δ_{Tropo}), we show the values of the differential total tropospheric delay, derived from radiosonde data and computed for the satellite incidence angle of each interferogram used on this study.

3.3 *Geophysical interpretation*

Having proved the minor influence of the atmosphere and the topography on the study area, we now turn to the interpretation that the fringe observed in the co-seismic interferograms is due to the earthquake. To identify the possible variability of refractivity in the radar signal we analysed the range change values extracted from six profiles drawn over the NW region of Pico. These profiles were drawn

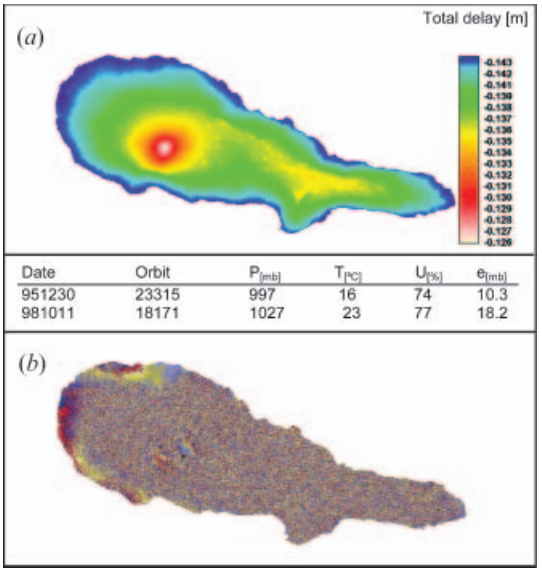

Figure 4. (*a*) Simulated troposphere interferogram computed using Saastamoinen–Mendes and Langley model. Meteorological data used for this computation were acquired on 30 December 1995 and on 11 October 1998, at FAIM site. (*b*) Differential SAR interferogram 951230–981011, after tropospheric correction.

across the best-correlated area of Pico Island, close to the main villages, where the slopes are not too steep, the agricultural fields are scarce and the ground cover is mostly volcanic rocks. These profiles are no more than 5 km long because phase decorrelates quickly with distance from the coast.

Reversals and autocorrelations are not considered in this analysis. Therefore, the minimum number of pairs required to capture all the geophysical deformation between the epochs of the first and last images is $k=p-1$, for p different epochs ($p \geqslant 2$, $p \in \mathrm{N}$) (Kohlhase *et al.* 2003). On the first column of table 3 the P, C and O characters identify the independent pairs used to study the pre-, co- and post-seismic periods, respectively.

In figure 5, we show averaged range change profiles corresponding to tracks 52 and 281. These are pre-seismic (mean obtained from five pairs corresponding to track 52 and five to track 281), co-seismic (mean obtained from seven pairs corresponding to track 52 and five to track 281) and post-seismic (a single profile from track 281). Mean phase profiles were unwrapped as 1-dimentional signals, converted to millimetres and shifted to the same origin (zero). Profiles were also compensated from differential total tropospheric delay computed for each interferometric pair.

Observing the profiles in figure 5 we conclude that there is no significant range shifts in the pre-seismic period. This fact is more evident in track 52, because geometric correlation between images of this track is higher than the correlation verified between images of track 281. This situation is clearly different in the co-seismic period, where the signal is larger and coherent along the profile. The maximum range change value reaches 30 mm in profile 4 of track 52. The strongest co-seismic deformation observed correspond to the area between profiles 3 and 5 (i.e. 369.9 km and 371.4 km, in the UTM easting direction). The maximum of deformation field is located approximately 3.5 km from the north coast (i.e. 4265.5 km and 4269.0 km, in the UTM northing direction).

The correlation of the unique post-seismic pair is poor, due its long orbital separation (Ha $= -19$ m). Yet, we can observe on panels of figure 5 some similarity between pre- and post-seismic profiles, suggesting that no significant range shifts occurred in the observed post-seismic period.

Mean co-seismic profiles described above are now compared with the modelled range shift profiles, calculated using Fernandes *et al.* (2002) fault parameters. In figure 6 we plot the elastic displacement associated with the two mechanisms proposed (Model 1 and Model 2, see figure 2), the mean co-seismic profiles 3, 4 and 5 and the standard deviation computed along the profile. Elastic displacement is computed using RNGCHN routine (Feigl and Dupré 1999, Okada 1985). Maximum range change observed is 29 mm, for profile 4 of track 52. Uncertainty associated with this measurement is expressed by the standard deviation on the mean and corresponds to 10 mm.

We can conclude that the displacement field depicted by InSAR matches the deformation envelope defined by the models obtained from GPS analysis (Fernandes *et al.* 2002) but cannot discriminate between them.

4. Discussion and conclusions

We have applied the differential InSAR technique to ERS data, acquired between 1992 and 2000, to analyse surface deformation produced by the 9 July 1998 earthquake. From a total of 17 available ERS images in descending mode, 12

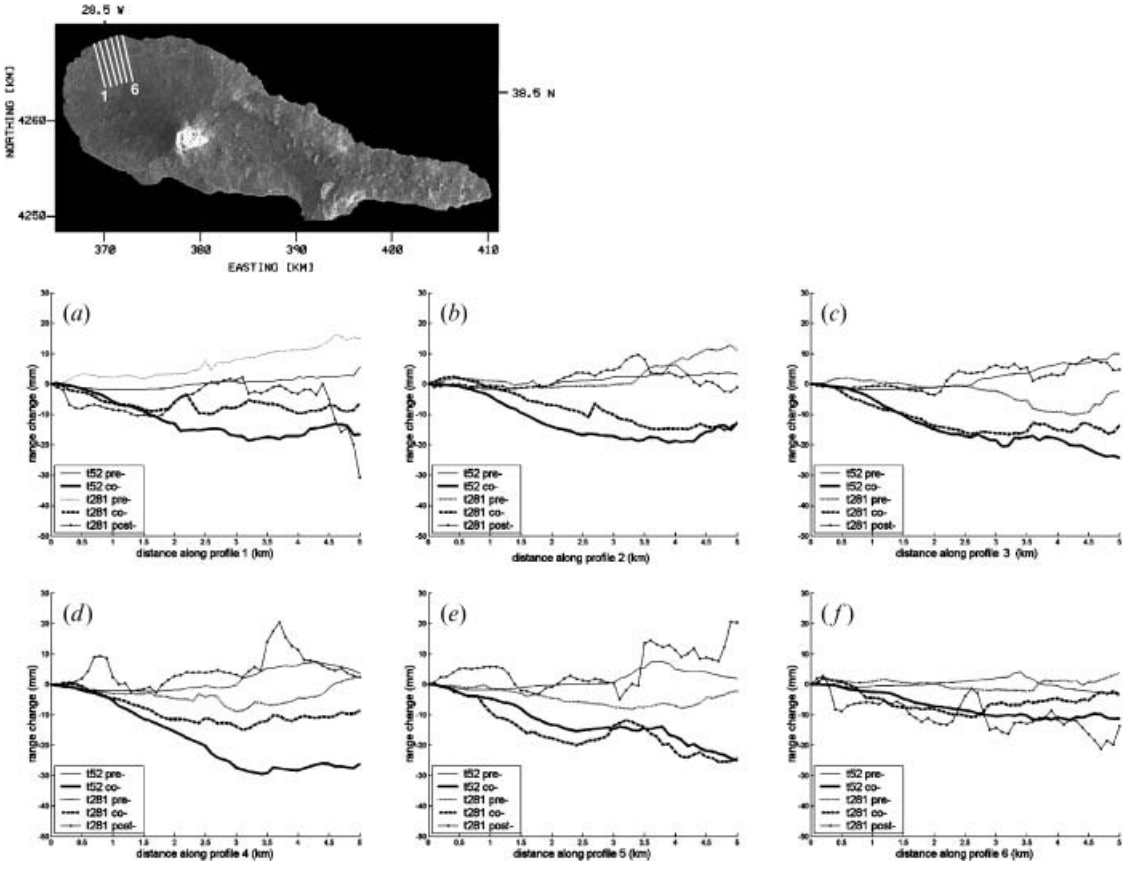

Figure 5. Amplitude image of Pico Island and profiles used on time series analysis. Panels A to F, show averaged range change profiles corresponding to tracks 52 and 281. Panels show, for both tracks, mean profiles obtained from the pre-, co- and post-seismic groups. Range change values are expressed in mm.

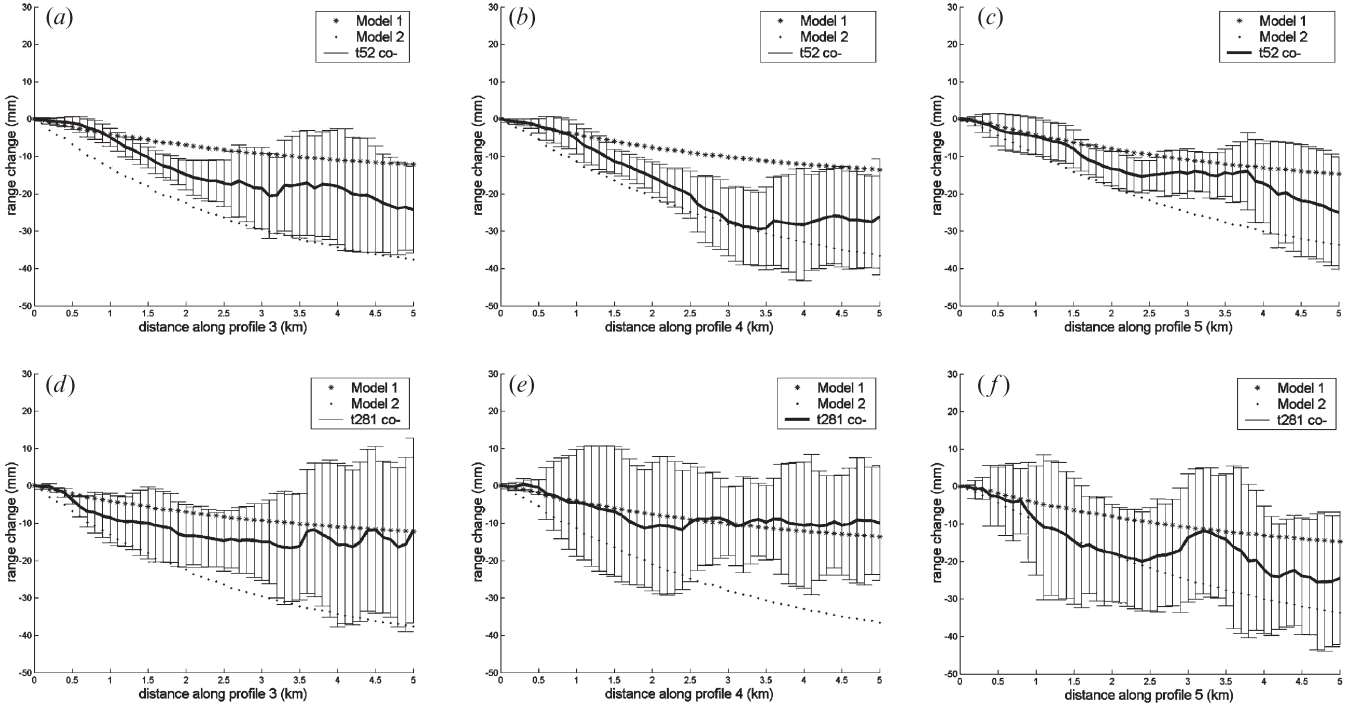

Figure 6. Comparison between modelled range shift profiles, associated with the two mechanisms (Model 1 and Model 2), and the mean co-seismic profiles 3, 4 and 5. Panels A, B and C refer to track 52 and panels D, E and F to track 281. Standard deviation computed along profile is also showed as error bars.

co-seismic interferograms were produced. We find fringe patterns with approximately 3 cm of range change between 1992 and 1998. Although correlation breaks down in most areas, the fringe pattern is legible on the NW part of Pico Island.

When we compare the amplitude and the spatial distribution of deformation with a synthetic model computed from the fault parameters of Fernandes *et al*. (2002) we conclude that the observed interferometric fringes generally agree with the synthetic models and, therefore, are coherent with the available seismological and GPS data.

The Azores islands are in an area where tectonic and volcanic activity is known to occur, generating significant surface deformation. However, the present knowledge of this deformation pattern is scarcely known. Only Furnas volcano (Sigmundsson *et al*. 1995) and Faial (Fernandes *et al*. 2002) have been the subject of detailed deformation studies. In the case of Faial only elastic co-seismic deformation was retrieved. Consequently, new studies and larger image sets are needed to address the inter-seismic deformation pattern in the Azores.

This was the first attempt to apply differential InSAR to the evaluation of ground displacement in the Azores. Results obtained are limited if we compare with similar studies developed for most of the well-known volcanic systems. The Azores geologic environment, characterized by a group of isolated islands, where expected ground displacements are reasonably small, is not the ideal candidate for InSAR. Available image pairs are scarce and statistical approaches like stacking are not feasible. Our study suffers from all these limitations; however, we can still identify interferometric signatures that are most probably of tectonic origin. Time series analysis seems to be a useful complement for direct inspection of interferometric fringes and we can anticipate that a larger number of image pairs can give us the required information to allow robust evaluations of the displacement pattern. Results presented here allow us to conclude that InSAR techniques coupled with GPS observations (which are now made on a regular basis in the Azores Islands) can give a valuable contribution to studies of the spatial distribution of the deformation field, unless the new radar sensors, like ENVISAT, provide new, additional information for geodynamic research.

Acknowledgements

This work was funded by FCT/SARAÇORES project (POCTI/CTA/36281/99). ERS images were acquired in the scope of the ESA project 1074-OD. We would like to thank the Instituto Geográfico do Exército, which provided the DEM, as well as Instituto de Meteorologia for supplying the meteorological data. This work benefited from useful comments by Virgilio Mendes, regarding the atmospheric delay in radio signal propagation. Comments from both anonymous reviewers improved the manuscript. This work constitutes also a contribution to the RETINA EU Project (EVG1-CT-2001-00046).

References

Afonso, A., Gomes, F. and Fernandes, M., 2002, IGeoE: Cartografia de qualidade – a base de um SIG. *Tribuna das Autarquias*, N., **108**, pp. 13–14.

Delacourt, C., Briole, P. and Achache, J., 1997, Tropospheric correction of the SAR interferograms with strong topography. Application to Etna. *Geophysical Research Letters*, **25**, pp. 2849–2852.

Dziewonski, A.M., Ekstrom, G. and Maternovskaya, N.N., 1999, Centroid-moment tensor solutions for July–September, 1998. *Physics of the Earth and Planetary Interiors*, **114**, pp. 99–107.

Feigl, K.L., 2002, Estimating earthquake source parameters from geodetic measurements. Vol. 81A. In *International Handbook of Earthquake and Engineering Seismology*, W.H.K. Lee, P.C. Jennings, H. Kanamori and C. Kisslinger (Eds), pp. 607–620 (Amsterdam, The Netherlands: Academic Press).

Feigl, K. and Dupré, 1999, RNGCHN: A program to calculate displacement components from dislocations in an elastic half-space with applications for modeling geodetic measurements of crustal deformation. *Computers and Geosciences*, **25**, pp. 695–704.

Feigl, K., Sergent, A. and Jacq, D., 1995, Estimation of an earthquake focal mechanism from a satellite radar interferogram: Application to the December 4, 1992 Landers aftershock. *Geophysical Research Letters*, **22**, pp. 1037–1040.

Fernandes, R.M.S., Miranda, J.M., Catalão, J., Luis, J.F., Bastos, L. and Ambrosius, B.A.C., 2002, Coseismic Displacements of the Mw=6.1, July 9, 1998, Faial Earthquake (Azores, North Atlantic). *Geophysical Research Letters*, **29**(16), 21-1–21-4.

Gaspar, J., Ferreira, T., Queiroz, G., Malheiro, A., Coutinho, R. and Trota, A., 1998, Avaliação dos perigos geológicos na ilha do Faial após o terramoto de 1998: o caso da Freguesia da Ribeirinha. *Proceedings of 1° Simpósio de Meteorologia e Geofísica da APMG*, 23–25 November 1998, Lagos, Portugal (Lisboa, Portugal: APMG), pp. 89–94.

Goldstein, R., 1995, Atmospheric limitations to repeat-track radar interferometry. *Geophysical Research Letters*, **22**, pp. 2517–2520.

Goldstein, R.M. and Werner, C.L., 1998, Radar interferogram filtering for geophysical applications. *Geophysical Research Letters*, **25**, pp. 4035–4038.

Hanssen, R.F., 2001, *Radar Interferometry Data Interpretation and Error Analysis* (Dordrecht, The Netherlands: Kluwer Academic).

Hanssen, R.F., Weckwerth, T.M., Zebker, H.A. and Klees, R., 1999, High-resolution water vapor mapping from interferometric radar measurements. *Science*, **283**, pp. 1295–1297.

Klinger, Y., Michel, R. and Avouac, J.-P., 2000, Co-seismic deformation during the Mw 7.3 Aqaba earthquake (1995) from ERS-SAR interferometry. *Geophysical Research Letters*, **27**, pp. 3651–3654.

Kohlhase, A.O., Feigl, K.L. and Massonnet, D., 2003, Applying differential InSAR to orbital dynamics: a new approach for estimating ERS trajectories. *Journal of Geodesy*, **77**, pp. 493–502.

Madeira, J., Brum, A. and Serralheiro, A., 1998, A tectónica do Faial e o sismo de 9 de Julho de 1998. *Proceedings of 1° Simpósio de Meteorologia e Geofísica da APMG*, 23–25 November 1998, Lagos, Portugal (Lisboa, Portugal: APMG), pp. 81–88.

Massonnet, D. and Feigl, K.L., 1995a, Satellite radar interferometric map of the coseismic deformation field of the M = 6.1 Eureka Valley, Calfornia earthquake of May 17, 1993. *Geophysical Research Letters*, **22**, pp. 1541–1544.

Massonnet, D. and Feigl, K.L., 1995b, Discrimination of geophysical phenomena in satellite radar interferogram. *Geophysical Research Letters*, **22**, pp. 1537–1540.

Massonnet, D. and Feigl, K.L., 1998, Radar interferometry and its application to changes in the Earth's Surface. *Reviews of Geophysics*, **36**, pp. 441–500.

Massonnet, D. and Rabaute, T., 1993, Radar interferometry: limits and potential. *IEEE Transactions on Geoscience and Remote Sensing*, **31**, pp. 455–464.

Massonnet, D., Rossi, M., Carmona, C., Adragna, F., Peltzer, G., Feigl, K. and Rabaute, T., 1993, The displacement field of the Landers earthquake mapped by radar interferometry. *Nature*, **364**, pp. 138–142.

Mendes, V.B. and Langley, R.B., 1998, Tropospheric zenith delay prediction accuracy for airborne GPS high-precision Positioning. *Proceedings of The Institute of Navigation*

54th Annual Meeting, 1–3 June 1998, Denver, CO, USA (Washington, D.C.: The Institute of Navigation), pp. 337–347. Available online at: http://mat.fc.ul.pt/eg/lattex/ion54am_ml.pdf (accessed 20 January 2004).

MENDES, V.B. and LANGLEY, R.B., 2000, An analysis of high-accuracy tropospheric delay mapping functions. *Physics and Chemistry of the Earth, Part A*, **25**, pp. 809–812.

MURAKAMI, M., TOBITA, M., SAITO, T. and MASHARU, H., 1996, Coseismic crustal deformations of the 1994 Northridge, California earthquake detected by interferometric analysis of SAR images acquired by the JERS-1 satellite. *Journal of Geophysical Research*, **101**, pp. 8605–8614.

NISHIMURA, T., FUJIWARA, S., MURAKAMI, M., TOBITA, M., NAKAGAWA, H., SAGIYA, T. and TADA, T., 2001, The M6.1 Earthquake triggered by volcanic inflation of Iwate volcano, northern Japan, observed by satellite radar interferometry. *Geophysical Research Letters*, **28**, pp. 635–638.

OKADA, Y., 1985, Surface deformation to shear and tensile faults in a half space. *Bulletin of the Seismological Society of America*, **75**, pp. 1135–1154.

ROSEN, P.A., HENSLEY, S., ZEBKER, H.A., WEBB, F.H. and FIELDING, E.J., 1996, Surface deformation and coherence measurements of Kilauea Volcano, Hawaii, from SIR-C radar interferometry. *Journal of Geophysical Research*, **101**, pp. 23109–23125.

SAASTAMOINEN, J., 1972, Contributions to the theory of atmospheric refraction. *Bulletin Geodesique*, **105**, pp. 106.

SANDWELL, D.T., SICHOIX, L., AGNEW, D., BOCK, Y. and MINSTER, J.-B., 2000, Near real-time radar interferometry of the Mw 7.1 Hector Mine Earthquake. *Geophysical Research Letters*, **27**, pp. 3101–3104.

SCHARROO, R. and VISSER, P., 1998, Precise orbit determination and gravity field improvement for the ERS satellites. *Journal of Geophysical Research*, **103**, pp. 8113–8127.

SENOS, M.L., GASPAR, J.L., CRUZ, J., FERREIRA, T., NUNES, J.C., PACHECO, J., ALVES, P., QUEIROZ, G., DESSAI, P., COUTINHO, R., VALES, D. and CARRILHO, F., 1998, O terramoto do Faial de 9 de Julho de 1998. In *1° Simpósio de Meteorologia e Geofísica da APMG*, 23–25 November 1998, Lagos, Portugal (Lisboa, Portugal: APMG), pp. 61–67.

SIGMUNDSSON, F., TRYGGVASON, E., ALVES, M.M., ALVES, J.L., PALSSON, K. and OLAFSSON, H., 1995, Slow inflation of the Furnas volcano, Sao Miguel, Azores, suggested from initial levelling and global positioning system measurements. *Geophysical Research Letters*, **22**, pp. 1681–1684.

TARAYRE, H. and MASSONNET, D., 1996, Atmospheric propagation heterogeneities revealed by ERS-1. *Geophysical Research Letters*, **23**, pp. 989–992.

WRIGHT, T.J., FIELDING, E.J., PARSONS, B.E. and ENGLAND, P.C., 2001, Triggered slip: observations of the 17 August 1999 Izmit (Turkey) earthquake using radar interferometry. *Geophysical Research Letters*, **28**, pp. 1079–1082.

ZEBKER, H.A., ROSEN, P.A. and HENSLEY, S., 1997, Atmospheric artifacts in interferometric synthetic aperture radar surface deformation and topographic maps. *Journal of Geophysical Research*, **102**, pp. 7547–7563.